Numerical simulation of scalar mixing from a point source over a wavy wall

By R. Rossi† AND G. Iaccarino

1. Motivation and objectives

The mixing of transported scalars in turbulent flows is a classic topic in turbulence research. The "diffusing power" of turbulent flows was originally recognized, among others, by Taylor (1915) since the beginning of the last century. Later on, Taylor (1921, 1935) also provided the first statistical framework to predict turbulent diffusion in air streams, as well as the scalar mixing in pipe flows (Taylor 1953, 1954). Although such fundamental work still forms the basis for the theoretical analysis of turbulent diffusion, over the last fifty years laboratory experiments and numerical simulations have profoundly advanced the understanding of the mixing process occurring in turbulent flows. An excellent review of this topic has recently been presented by Dimotakis (2005), while the recent achievements in passive scalars mixing, when flow dynamics proceeds independently from the mixing process, can be found in Warhaft (2000).

Among the several flow phenomena relevant to the analysis of turbulent mixing, our attention and research efforts are directed towards the modeling of scalar dispersion from localized sources in complex flows (Rossi & Iaccarino 2009*b*). The present analysis is motivated by the need to obtain a deeper insight into turbulent mixing occurring in the presence of complex flow features, which may severely affect the reliability of simplified theoretical and numerical models. For example (Rossi & Iaccarino 2008), the analysis of scalar dispersion from a line source downstream of a square obstacle has clarified that gradient-transport models based on the Standard Gradient-Diffusion Hypothesis (SGDH) are unable to predict the streamwise component of scalar fluxes. On the other hand, a preliminary evaluation of refined gradient-transport closures for the same flow setup (Rossi & Iaccarino 2009*a*) suggests that Algebraic Flux Models (AFMs) yield reasonable predictions of the scalar flux anisotropy. However, the limited amount of experimental data for the obstacle flow made it difficult to perform a meaningful and comprehensive validation of algebraic closures.

The release of a passive tracer from a point source over a wavy wall is adopted in this work to investigate the scalar mixing over complex topography using Direct Numerical Simulations (DNS). It is worth noting that a comparative analysis of low-order statistics against the present DNS data (Rossi 2009*b*) established that algebraic flux models are able to capture the complex development of scalar fluxes in the far field over the wavy boundary, but not in the neighborhood of the source. Here, we intend to provide a deeper insight into the physics of the scalar mixing process as well as some of the rationale behind the capabilities and limitations of algebraic closures.

† Laboratorio di Termofluidodinamica Computazionale, Seconda Facoltà di Ingegneria di Forlì, Università degli Studi di Bologna, Via Fontanelle 40, 47100 Forlì, Italy

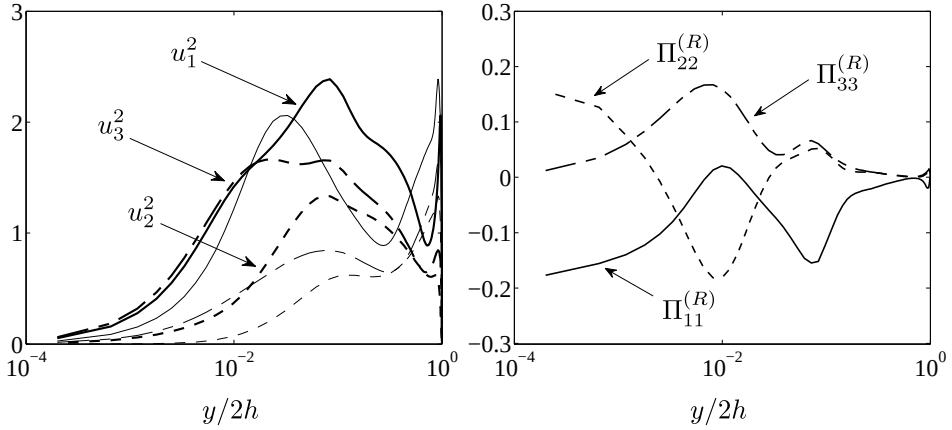

FIGURE 1. Some examples of distinguishing features of flows over wavy surfaces: left panel, wavelength-averaged profiles of velocity R.M.S., thin lines show the corresponding profiles at the flat plate; right panel, pressure-strain contributions to normal turbulent stresses on the upslope side of the wave.

2. Distinguishing features of flows over wavy surfaces

The flow over wavy surfaces has been extensively adopted to mimic the interaction of air streams with complex geometry. Examples consist of thermal convection in the lower part of the atmosphere (Krettenauer & Schumann 1992), the gas-liquid interaction over water waves (Fulgosi *et al.* 2003) or the enhancement of forced convection under laminar (Fabbri & Rossi 2005) and turbulent (Rossi 2006) conditions.

The effect of surface wavyness is essentially felt by turbulence through the production term in the Reynolds stress equation:

$$P_{ij}^{(R)} \equiv -R_{ik}\frac{\partial U_j}{\partial x_k} - R_{jk}\frac{\partial U_i}{\partial x_k}\,, \tag{2.1}$$

The additional mean rate of strain induced by the wave is responsible for increasing the rate of production of streamwise velocity fluctuations, as well as determining the direct production of vertical turbulent fluctuations (Hudson *et al.* 1996). However, the wavelength-averaged profiles of turbulence intensities, shown in Fig. 1, do not only highlight the marked increased of the vertical turbulence intensity. In fact, the spanwise component undergoes a stronger enhancement compared to the vertical velocity.

Since lateral velocity fluctutations cannot be directly produced due to the spanwise homogeneity of the flow, the wavy surface must also be responsible for increasing the energy transfer between velocity components. This can be clarified by looking at the pressure-strain term in the Reynolds stress equation:

$$\Pi_{ij}^{(R)} \equiv -\overline{\frac{1}{\rho}p\left(\frac{\partial u_i}{\partial x_j} + \frac{\partial u_j}{\partial x_i}\right)}\,, \tag{2.2}$$

For an incompressible flow $\Pi_{ii}^{(R)} = 0$ and $\Pi_{ij}^{(R)}$ acts to redistribute the energy between velocity fluctuations. In Fig. 1, the vertical profiles of pressure-strain terms arising in the equation for the normal stresses are plotted on the upslope side of the wave, where the lateral turbulence intensity shows a maximum at the wall. Although the $\Pi_{33}^{(R)}$ term goes to zero toward the surface, immediately further away from the wall the energy transfer from

A/λ	H/A	$L \times 2h \times W$	$N_x \times N_y \times N_z$	$\Delta x^+ \times \Delta y^+ \times \Delta z^+$	D_s^+	u_w^*	Re_h^*	Sc
0.05	13	$4\lambda \times \lambda \times 2\lambda$	$256 \times 96 \times 128$	$9.6 \times 0.09 - 2.9 \times 9.6$	22.5	0.09	300	1

TABLE 1. Summary of flow and numerical parameters.

the vertical (negative) term to the lateral (positive) component is significant. De Angelis *et al.* (1997) argued that such a mechanism is controlled by *splat* and *anti-splat* events (Perot & Moin 1995) which give rise to a different unbalance in $\Pi_{ij}^{(R)}$. This phenomenon is similar to the flow impingement over a blocking wall, where in general splats occur owing to kinematic constraints over the surface. For reasons of continuity, anti-splats must form and the balance between splats and anti-splats is dictated by the dissipation over the surface. Later on however, Henn & Sykes (1999) also reported large values of lateral fluctuations in the case of non-separated conditions using large-eddy simulations. They concluded that a possible mechanism in the production of u_3^2 can be the Taylor-Göertler instability (Göertler 1941); however, this scenario has not been clarified yet.

3. Flow and numerical setup

The numerical experiment consists of the release of a passive tracer from a point source in a two-dimensional channel composed of a flat plate and a wavy surface. The general setup and a sketch of flow and boundary conditions is shown in Fig. 2. The wavy profile is prescribed by the following function:

$$y_w = A\left(\cos\frac{2\pi x}{\lambda}\right), \tag{3.1}$$

where A denotes the wave amplitude and λ denotes the profile wavelength. The wave steepness $2A/\lambda$=0.1 and the Reynolds number adopted in the computations are such that flow separation is observed in the region $0.13 \leq x/\lambda \leq 0.62$ of each wave (see Fig.2), in agreement with other DNS studies (Maaβ & Schumann 1994). The flow is assumed to be fully-developed, thus periodic conditions are applied in the streamwise as well as along the spanwise directions.

The source is located at x/λ=1, on top of the wave crest. Although the source size is of no importance in the case of a ground release (Fackrell & Robins 1982), it should be noted that the occurrence of flow separation downstream of the source may alter this scenario. However, here the effect of the source size D_s has not been investigated yet. The scalar injection rate relative to the mass flow rate in the channel is of the order of numerical accuracy for the mass conservation (10^{-6}). Therefore, it can be considered a negligible contribution to the streamwise periodicity of the flow. The overall flow and numerical parameters are reported in Tab. 1. Note that wall-units are computed from the reference velocity $u_w^* = \sqrt{\Pi_p h/\rho}$, which is based on the constant pressure-gradient Π_p driving the flow and the average channel half-width h.

The flow and scalar governing equations are numerically solved using unstructured finite-volume schemes. The solution is advanced in time using a fully-implicit second-order accurate time-stepping method, while the pressure-velocity decoupling due to variable co-location is controlled by the dissipation scheme of Rhie & Chow (1983). A low-order symmetric central interpolation opearator is adopted for the convective term of the

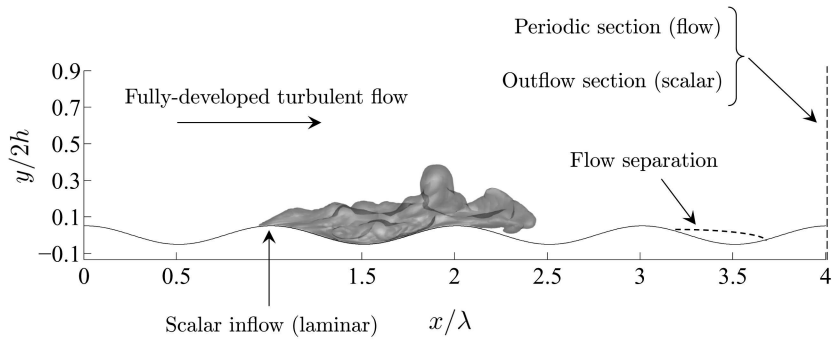

FIGURE 2. Sketch of flow and boundary conditions for the present study.

momentum equation to improve the accuracy in computing the momentum turbulence (Mahesh *et al.* 2004), while the very sharp interface arising at the edge of the scalar plume forced the introduction of an upwind-biased scheme for the advection term of the scalar transport equation.

The scalar variable is thus interpolated at cell-faces using the following one-sided linear reconstruction:

$$C(x,y) = C(x_0,y_0) + \alpha \frac{\partial C}{\partial x_i}\Big|_0 R_i\,, \tag{3.2}$$

where R_i is the displacement vector from the cell centroid to any point within the cell volume. The slope-limiter technique developed by Barth & Jespersen (1989) is employed to keep the linear reconstruction bounded within the local extrema of the scalar field. The limiter is computed over each cell face as follows:

$$\alpha_f = \begin{cases} \min\left(1, \frac{C_{\max}-C_0}{C_f-C_0}\right) & \text{if } (C_f - C_0) > 0 \\ \min\left(1, \frac{C_{\min}-C_0}{C_f-C_0}\right) & \text{if } (C_f - C_0) < 0\,, \\ 1 & \text{otherwise} \end{cases} \tag{3.3}$$

and finally set as $\alpha = \min(\alpha^f)$. Although similar techniques have also been employed in other DNS studies of turbulent mixing (Brethouwer *et al.* 1999), the non linear character of the slope-limiting procedure may considerably affect the spectrum of scalar fluctuations (Rossi 2009*a*) and this should be kept in mind in the analysis of turbulence statistics, especially when these are related to the rate of scalar dissipation.

The computational grid is composed of hexahedral cells uniformly distributed along the streamwise and spanwise homogeneous directions, while hyperbolic stretching is applied between the wavy surface and the flat plate. No-slip and zero-flux conditions are applied at the solid boundaries. Note that the coefficients of the discrete scalar transport equation are properly modified at periodic boundaries to achieve a convective outlet condition for the scalar plume (see Fig. 2).

4. Results

In this section we present turbulence statistics computed by time-averaging statistical samples collected every t^+=6.35 × 10^{-3} time units, where $t^+ = tu_w^*/h$, for a total integration time of t^+=190. The results are compared to measurements of dispersion from elevated (ES) and ground (GS) sources over a flat plate performed by Fackrell & Robins

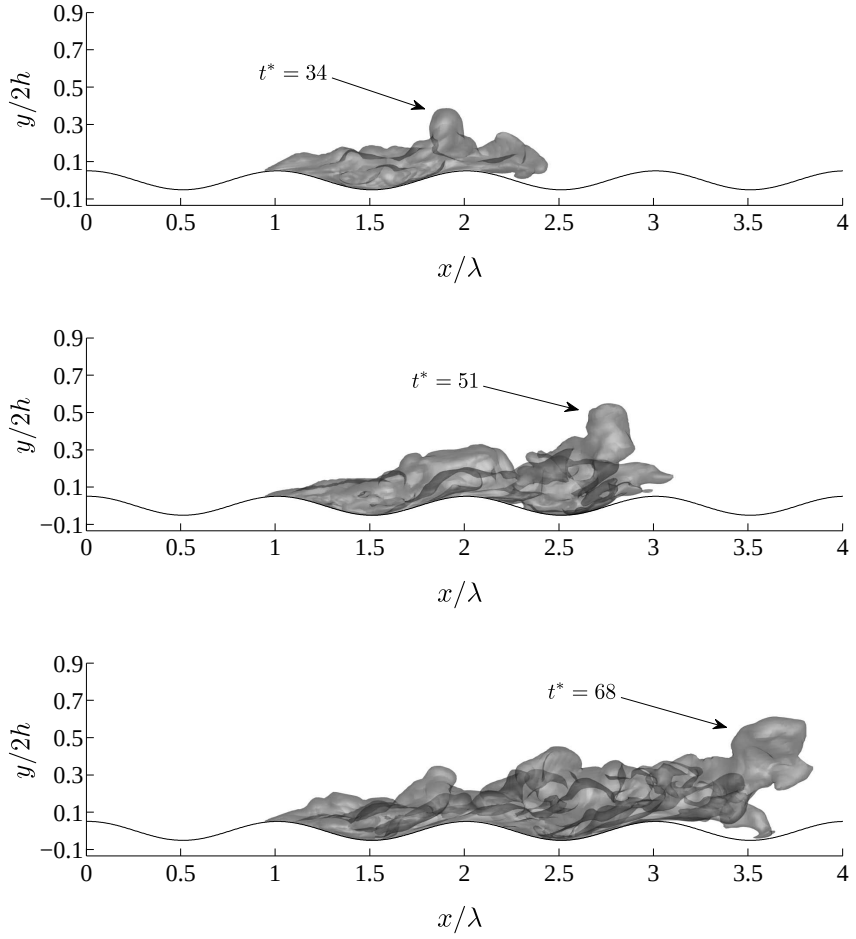

FIGURE 3. Structure of the instantaneous scalar plume above the wavy wall as a function of normalised time units $t^* = tU/H$; the arrow highlights the eduction of one large-scale structure at the wave upslope (upper panel) and tracks the subsequent development and entrainment of the structure in the bulk of the flow.

(1982). Note that, for the sake of brevity, the following analysis is limited to the scalar field. For a detailed discusssion of flow field results and the validation of the numerical technique, the reader is referred to Rossi (2006).

4.1. *Structure of the scalar plume*

The structure of the scalar plume at early development stages is presented in Fig. 3. The effect of flow separation occuring over the first half of the profile wavelength can be clearly noticed in Fig. 3(a), where the scalar plume detaches from the wall at $x/\lambda \geq 2$. The figure also highlights the eduction of one large-scale structure, originating at the wave upslope, which is probably connected with abrupt ejections of fluid from the wave trough toward the center of the channel (Cherukat *et al.* 1998). The shape of such a structure is essentialy preserved over one wavelength downstream, as shown in Fig. 3(b), corresponding approximately to 17 normalised time-units t^*=tU/H. The macroscopic

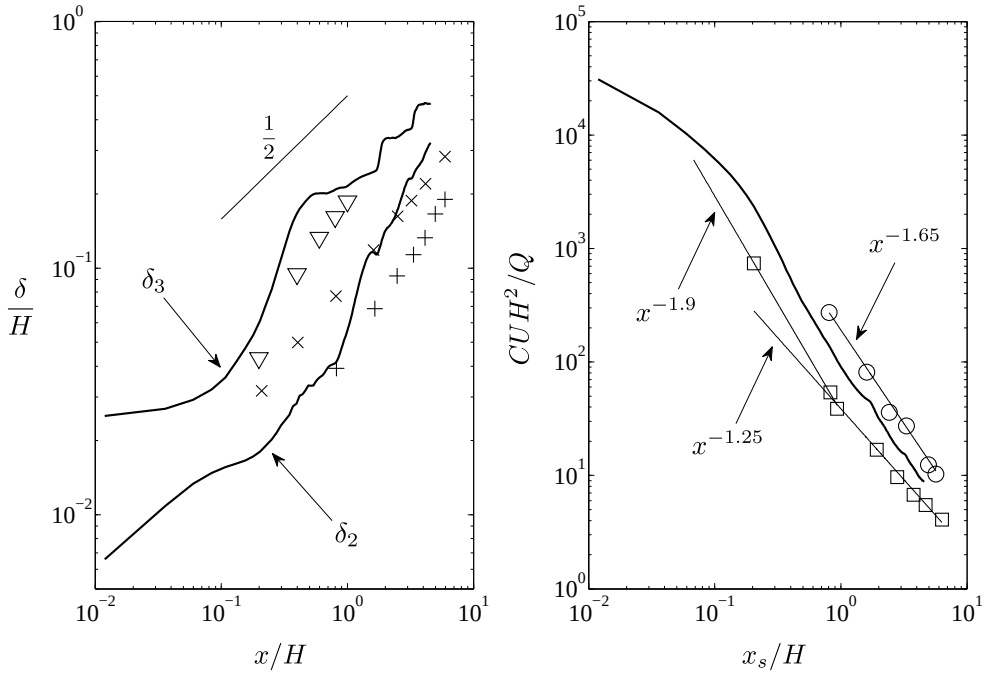

FIGURE 4. Vertical (δ_2) and lateral (δ_3) plume widths (left panel) and maximum concentration (right panel) over the wavy wall: +, ×, vertical and lateral plume widths from Fackrell & Robins (1982), Re_H≈270,000; ▽, lateral plume width from Wagner *et al.* (2007), Re_H≈18,000; ○, □, maximum concentration downstream elevated and ground sources from Fackrell & Robins (1982), Re_H≈270,000.

mixing of the blob appears to initiate after one subsequent time-interval of similar extent, when the initial development of another structure can be noted at $x/\lambda \approx 2$ in Fig. 3(c).

4.2. *Mean scalar concentration*

The spatial development of the mean scalar field is quantified in Fig. 4 by plotting the vertical and lateral plume width, defined as the location where the mean concentration is half of the local corresponding maximum value. Note that the vertical spread refers to $y = 0$ and the lateral spread is computed at the ground, $y = y_w$. In order to compare our DNS results with measurements, the plume spread and the distance from the source x_s are normalised by the equivalent boundary layer thickness in the channel, H, defined as the wavelength-averaged vertical location of the maximum of streamwise velocity (see also Tab. 1). The vertical spread is initially close to the flat plate results. The slope significantly increases downstream of the first wave upslope, $x_s/H \approx 1.5$, and the vertical size of the plume is significanlty larger than over the flat plate. Since the Reynolds number of the computations is considerably lower compared to the experiments, the plume has certainly more time to diffuse. However, turbulent fluctuations and thus turbulent transport would be reduced at a lower Reynolds number over the flat plate. The wavy surface must thus be able to mitigate such reduction. The estimated lateral spread is also larger compared to the flat plate profile, while the slope is similar to the measurements for a wavy wall reported by Wagner *et al.* (2007). However, it is found much larger within the separated region, $0.2 \leq x_s/H \leq 0.95$, than at the wave upslope. Fig. 4 also shows

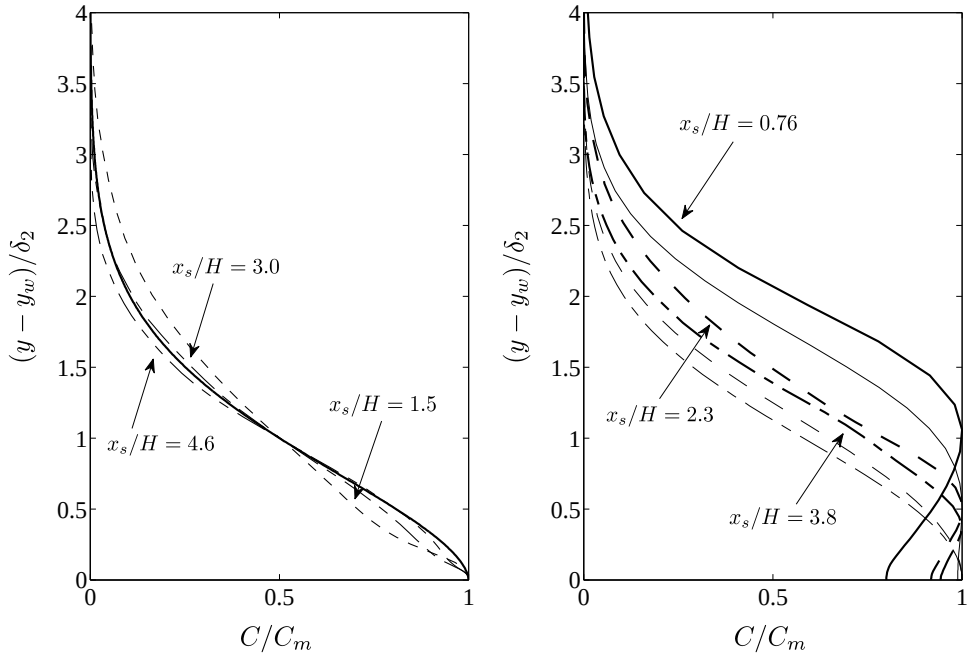

FIGURE 5. Vertical profiles of mean scalar concentration at the wave crest (left panel) and at the wave trough (right panel) above successive wave locations: the solid line on the left panel shows the empirical fit of Fackrell & Robins (1982); thin lines on the right panel shows the reflected Gaussian model (4.2).

the streamwise decay of maximum concentration. The rate of decay along the first wavelength seems to fit well with the initial slope for the elevated source reported by Fackrell & Robins (1982). In the far-field, the decay rate reduces toward the slope of the ground release. It is also interesting to note that the normalised maximum concentration profile lies between the GS and ES curves reported in the experiments.

The vertical profiles of mean concentration above the wave crests, shown in Fig. 5, seem to achieve self-similarity in the far field. At the last station available from the computational domain, $x_s/H = 4.6$, the profile is well described by the following empirical correlation (Robins 1978):

$$C = C_0 \exp\left\{-0.693(y/\delta_2)^s\right\}, \tag{4.1}$$

where the exponent $s = 1.7$ is taken from a rough boundary-layer experiment. The profiles above wave troughs are shown on the right panel of Fig. 5. Here the plume is separated from the wavy surface and qualitatively resembles the profiles of elevated sources. An empirical fit with the following reflected Gaussian model adopted in Fackrell & Robins (1982) has therefore been attempted:

$$C \sim \left\{\exp(-0.693(y + y_s)^2/\delta_2^2) + \exp(-0.693(y - y_s)^2/\delta_2^2)\right\}, \tag{4.2}$$

but none of the profiles seem to be reasonably described by such empirical formulae, even when some tuning of the parameters appearing in Eq. (4.2) is performed.

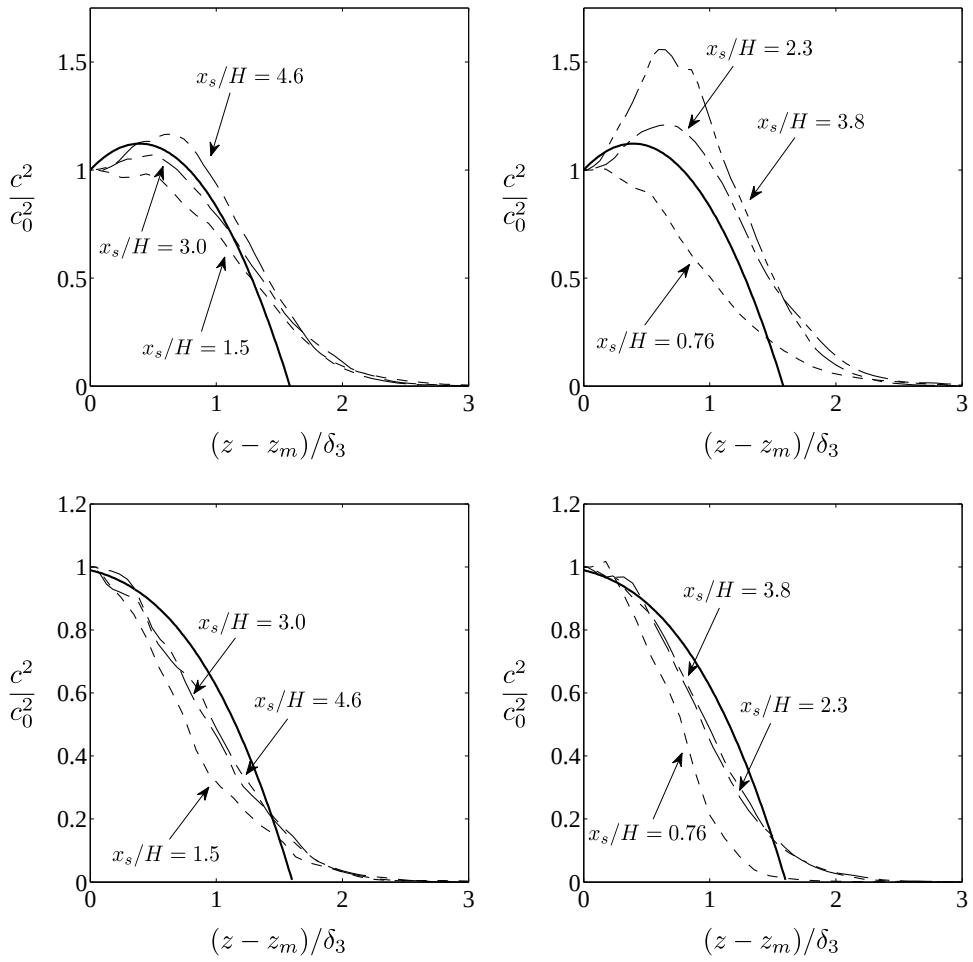

FIGURE 6. Lateral profiles of concentration R.M.S. at the wave crest (left panels) and at the wave trough (right panels) above successive wave locations; cross sections are taken at $y/\delta_2 \approx 0.5$ (upper panels) and $y/\delta_2 \approx 1.5$ (lower panels); the solid line shows the polynomial fit to experimental data of Fackrell & Robins (1982) at similar vertical locations and $x_s/H = 5.92$.

4.3. *Concentration fluctuations*

The lateral profiles of scalar fluctuations above the wavy surface are presented in Fig. 6 and compared to the flat plate measurements. An off-centre maxmimum can clearly be distinguished from the computed and measured profiles at similar locations below the vertical plume half-width δ_2. This is essentially determined by local production of scalar fluctuations, which is maximum at locations where the mean scalar gradient is the highest (Lavertu & Mydlarsky 2005). The off-centre maximum disappears at the first crest and trough close to the source, and similar results have been found in the case of the flat plate at $x_s/H = 0.85$. At the wave trough, the magnitude of normalised scalar fluctuations is much larger compared to experimental profiles. This indicates that the wavy surface leads to increased local production across the shear-layer originating from the separation point on the downhill side of the wave.

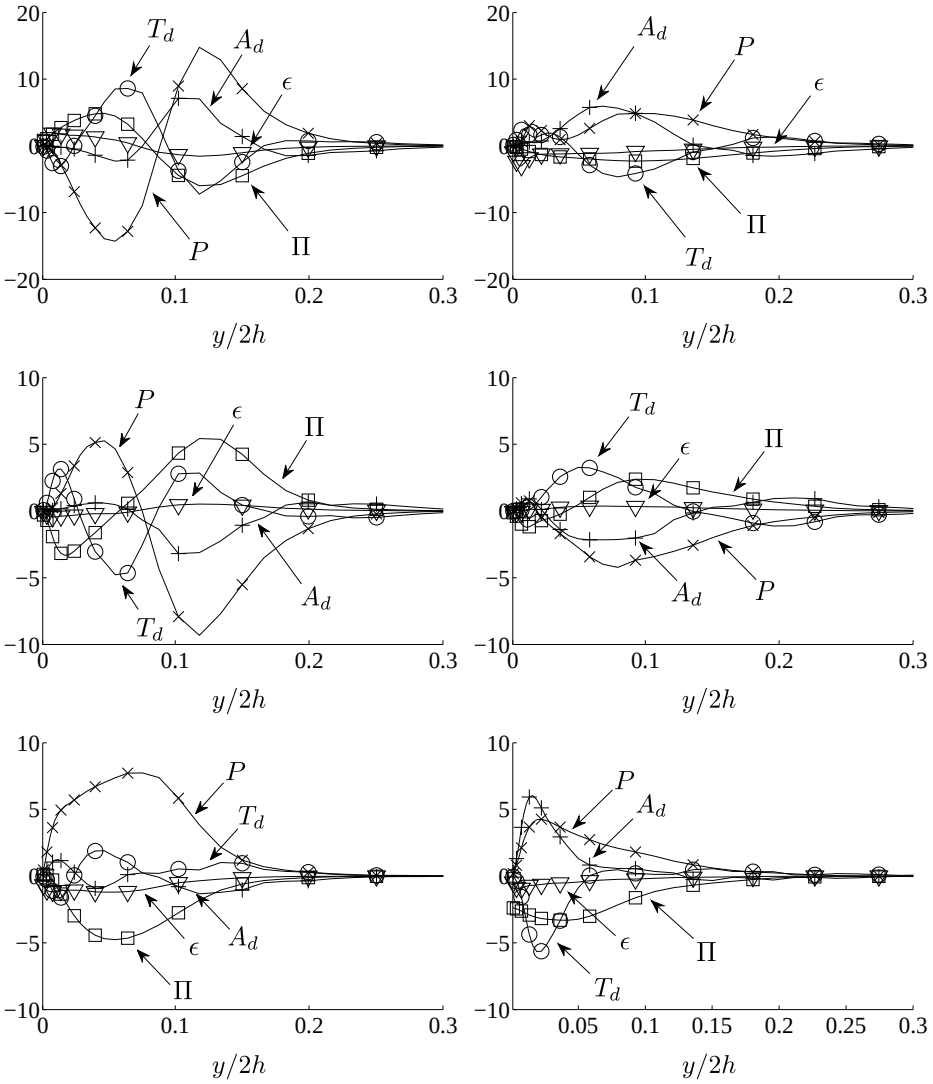

FIGURE 7. Budget of scalar fluxes at the first wave trough (left panels) and crest (right panels) downstream of the source: from top to bottom, $\overline{uc}$ budget, $\overline{vc}$ budget, $\overline{wc}$ budget; A_d, advection, P, production, Π, scalar-pressure-gradient correlation, T_d, turbulent diffusion, ϵ, dissipation.

4.4. *Budgets of scalar fluxes*

As the complexity of flow phenomena increases, some level of modeling must be introduced in order to ameliorate the computational effort required by numerical simulations. In the framework of heat and mass transport computations, it is customary to assume the scalar flux proportional to the mean scalar gradient, leading to *gradient-transport* type closure models. However, it should be noted that these type of closures are legitimate only when the budget of scalar fluxes is essentially dictated by a balance between the production term and pressure effects (Launder 1978). An inspection of scalar fluxes over the wavy surface is therefore presented to address the validity of the gradient-transport hypothesis in the present flow configuration.

The budget equation of scalar fluxes for a non-buoyant fluid reads as follows:

$$U_j \frac{\partial}{\partial x_j}\left(\overline{u_i c}\right) = -\left(\overline{u_i u_j}\frac{\partial C}{\partial x_j} + \overline{u_j c}\frac{\partial U_i}{\partial x_j}\right) - \frac{\partial}{\partial x_j}\left(\overline{u_j u_i c}\right) + \overline{\frac{c}{\rho}\frac{\partial p}{\partial x_i}} + \\ -\left(\nu\frac{\partial}{\partial x_j}\overline{c\frac{\partial u_i}{\partial x_j}} - D\frac{\partial}{\partial x_j}\overline{u_i\frac{\partial c}{\partial x_j}}\right) - (\nu + D)\,\overline{\frac{\partial u_i}{\partial x_j}\frac{\partial c}{\partial x_j}}, \tag{4.3}$$

where the advection by the mean flow appears on the left-hand side and the terms on the right-hand side denote production, turbulent diffusion, the scalar-pressure-gradient correlation, molecular diffusion and dissipation, respectively. Note that molecular diffusion has been found negligible in the present case and thus is not reported. Fig. 7 shows the scalar flux budgets above the first wave trough ($x/\lambda = 1.5$) and crest ($x/\lambda = 2$) downstream of the source. Each term in Eq. (4.3) is normalised by the friction velocity u_w^*, the local maximum concentration C_m, and the channel half-height h. Note that here the vertical coordinate is a measure of the distance from the wavy surface. It is also important to note that due to the inhomogeneity of the scalar field, the budgets have been computed only by time-averaging the local instantaneous values. As a consequence, the present profiles are not perfectly converged in the statistical sense. Nonetheless, it is possible to observe some interesting features from the inspection of DNS results.

The wavy surface has a significant impact on the streamwise flux budget, not previously reported in similar studies. In a simple-shear flow, the balance between production and dissipation prevails for this component (Kasagi *et al.* 1992). However, from Fig. 7 it is clear that dissipation is almost negligible in the present case, and production is essentially balanced by the scalar-pressure-gradient correlation and turbulent diffusion. A similar picture is found for the vertical flux, where turbulent diffusion dominates among the production-balancing terms within the separated region, while the scalar-pressure-gradient correlation is found more pronounced at $y/2h \geq 0.05$. The local-equilibrium between production and the scalar-pressure-gradient correlation required by gradient-transport closures seems satisfied to a larger extent in the case of the spanwise flux budget above the wave trough. At the wave crest and close to the surface however, turbulent diffusion as well as the mean flow advection are significant.

5. Summary and future work

We presented a DNS study of scalar mixing from a point source over a wavy wall. This particular flow configuration is found very useful in order to increase the complexity of the scalar mixing process and to maintain an accurate control over boundary conditions. The initial characterization of the scalar plume dispersal shows close similarity between the present results above the wave crests and dispersion from ground sources in smooth turbulent boundary layers. Major differences exist for mean concentration and concentration fluctuations over the wave trough, where the flow is separated and a strong shear-layer originates from the downhill side of the wave. The budget of scalar fluxes close to the source do not present a distinguished local-equilibrium between two-dominant terms. However, the lateral budget seems to be essentially dictated by the production and the scalar-pressure-gradient correlation, in agreement with the results from the *a-posteriori* test of algebraic flux models performed in Rossi (2009*b*). The established DNS database is now being further post-processed in order to present the *a-priori* analysis of the hy-

potheses which form the basis of algebraic models, aiming at clarifying the applicability of such closures to fully-inhomogenous flows.

Acknowledgments

The present work has been supported by the Marco Polo program of the University of Bologna. The support from the Army High-Performance Computing Research Center at Stanford University is also gratefully acknowledged.

REFERENCES

Barth, T. J. & Jespersen, D. C. 1989 The design and application of upwind schemes on unstructured meshes. AIAA Paper 89-0366.

Brethouwer, G., Boersma, B. J., Pourquié, M. B. J. M. & Nieuwstadt, F. T. M. 1999 Direct numerical simulation of turbulent mixing of a passive scalar in pipe flow. *Eur. J. Mech. B/Fluids* **18**, 739–756.

Cherukat, P., Na, Y., Hanratty, T. J. & McLaughlin, J. B. 1998 Direct numerical simulation of a fully developed turbulent flow over a wavy wall. *Theoret. Comput. Fluid Dyn.* **11**, 109–134.

De Angelis, V., Lombardi, P. & Banerjee, S. 1997 Direct numerical simulation of turbulent flow over a wavy wall. *Phys. Fluids* **9**, 2429–2442.

Dimotakis, P. E. 2005 Turbulent mixing. *Annu. Rev. Fluid Mech.* **37**, 329–356.

Fabbri, G. & Rossi, R. 2005 Analysis of the heat transfer in the entrance region of optimised corrugated wall channel. *Int. Comm. Heat Mass Transf.* **32**, 902–912.

Fackrell, J. E. & Robins, A. G. 1982 Concentration fluctuations and fluxes in plumes from point sources in a turbulent boundary layer. *J. Fluid Mech.* **117**, 1–26.

Fulgosi, M., Lakehal, D., Banerjee, S. & De Angelis, V. 2003 Direct numerical simulation of turbulence in a sheared air-water flow with a deformable interface. *J. Fluid Mech.* **482**, 319–345.

Goertler, H. 1941 Über eine dreidimensionale instabilität laminarer grenzschichten an konkaven wänden. *Z. angew. Math. Mech.* **21**, 250–252.

Henn, D. S. & Sykes, R. I. 1999 Large-eddy simulation of turbulent flow over wavy surface. *J. Fluid Mech.* **383**, 75–112.

Hudson, J. D., Dykhno, L. & Hanratty, T. J. 1996 Turbulent production in flow over a wavy wall. *Exps Fluids* **20**, 257–265.

Kasagi, N., Tomita, Y. & Kuroda, A. 1992 Direct numerical simulation of passive scalar field in a turbulent channel flow. *J. Heat Transf.-Trans. ASME* **114**, 598–806.

Krettenauer, K. & Schumann, U. 1992 Numerical simulation of turbulent convection over wavy terrain. *J. Fluid Mech.* **237**, 261–299.

Launder, B. E. 1978 Heat and mass transport. In Topics in Applied Physics ed. P. Bradshaw, pp. 231-287, Springer.

Lavertu, R. A. & Mydlarsky, L. 2005 Scalar mixing from a concentrated source in turbulent channel flow. *J. Fluid Mech.* **528**, 135–172.

Maaβ, C. & Schumann, U. 1994 Numerical simulation of turbulent flow over a wavy boundary. In Direct and Large-Eddy Simulation I ed. P. R. Voke, L. Kleiser & J. P. Chollet, pp. 287–297. Kluwer.

Mahesh, K., Constantinescu, G. & Moin, P. 2004 A numerical method for large-eddy simulation in complex geometries. *J. Comput. Phys.* **197**, 215–240.

Perot. B. & Moin, P. 1995 Shear free turbulent boundary layers. Part 1. Physical insight into near wall turbulence. *J. Fluid Mech.* **295**, 199–227.

Rhie, C. M. & Chow, W. L. 1983 A numerical study of the turbulent flow past an isolated airfoil with trailing edge separation. *AIAA J.* **21**, 1525–1532.

Robins, A. G. 1978 Plume dispersion from ground-level sources in simulated atmospheric boundary layers. *Atmos. Environ.* **12**, 1033-1044.

Rossi, R. 2006 Passive scalar transport in turbulent flows over a wavy wall. PhD thesis, Università degli Studi di Bologna, Bologna, Italy.

Rossi, R. 2009*a* Direct numerical simulation of scalar transport using unstructured finite-volume schemes. *J. Comput. Phys.* **228**, 1639–1657.

Rossi, R. 2009*b* A numerical study of algebraic flux models for heat and mass transport in complex flows. *Int. J. Heat Mass Transf.*, submitted.

Rossi, R. & Iaccarino, G. 2008 Numerical simulation of scalar dispersion downstream of a square obstacle. *Center for Turbulence Research, Annual Research Briefs*, pp. 287–312.

Rossi, R. & Iaccarino, G. 2009*a* Numerical simulation of scalar dispersion downstream of a square obstacle using gradient-transport type models. *Atmos. Environ.* **43**, 2518–2531.

Rossi, R. & Iaccarino, G. 2009*b* Computational aspects of scalar dispersion modeling and simulation in complex flows. *Nuovo Cimento Soc. Ital. Fis. C-Geophys. Space Phys.* **32**, 257–260.

Taylor, G. I. 1915 Eddy motion in the atmosphere. *Phil. Trans. R. Soc. Lond.* A **215**, 1–16.

Taylor, G. I. 1921 Diffusion by continuous movements. *Proc. R. Soc. Lond.* A **20**, 196–212.

Taylor, G. I. 1935 Statistical theory of turbulence. IV-Diffusion in a turbulent air stream. *Proc. R. Soc. Lond.* A **151**, 465–478.

Taylor, G. I. 1953 Dispersion of soluble matter in a solvent flowing slowly through a pipe. *Proc. R. Soc. Lond.* A **219**, 186–203.

Taylor, G. I. 1954 The dispersion of matter in turbulent flow through a pipe. *Proc. R. Soc. Lond.* A **223**, 446–68.

Wagner, C., Kuhn, S. & von Rohr, P. R. 2007 Scalar transport from a point source in flows over wavy walls. *Exp. Fluids* **43**, 261–271.

Warhaft, Z. 2000 Passive scalars in turbulent flows. *Annu. Rev. Fluid Mech.* **32**, 203–240.